Evaluation of MESFET Nonlinear Intermodulation Distortion Reduction by Channel-Doping Control

José Carlos Pedro, *Member, IEEE*

***Abstract*—This paper is intended to evaluate the linearity that can be provided by general-purpose MESFET's. By a simple physics-based analysis and a practical amplifier design, it will be shown how educated device and bias-point selection can approximate intermodulation distortion (IMD) performance of some normal channel-doping profiles, for which previous theories would not be able to predict good IMD performance, to the one expected from MESFET devices with specially tailored doping profiles.**

***Index Terms*— Doping profile, intermodulation, linearity, MESFET amplifier, Volterra series.**

I. Introduction

MANY are the telecommunications systems that require solid-state MESFET amplifiers capable of providing carrier to in-band intermodulation (C/I) distortion ratios as large as 50–70 dBc. Such figures usually impose voluminous, inefficient, and very expensive power-amplifier linearization schemes. A more reasonable, but also more demanding, approach tries to develop techniques capable of optimizing nonlinear intermodulation (IMD) performance of otherwise common power amplifiers. The main difficulty associated with that task is concerned with the poor understanding that one has of the circuit's IMD generation process. This, in turn, is mainly due to the lack of computer-aided design (CAD) aids appropriate to IMD simulation, and accurate enough MESFET nonlinear models and characterization procedures. Fortunately, in recent years, important developments in these areas have been reached [1]–[3], which encouraged this power-amplifier IMD optimization approach.

It is widely known that in highly linear amplifiers, nonlinear distortion products of third-order dominate the circuit's in-band IMD performance. To maintain IMD at reasonably low levels, their active devices are always biased for class-A operation, and the signal excursions kept small compared to the transistor's maximum allowed clipping-free signal range. This procedure prevents the appearance of a form of distortion, which in most cases manifests itself as soft clipping, and is imposed by the active device's strong nonlinearities (*I–V* curves' knees). However, in quasi-linear operation, the residual or mild nonlinearities of the drain–source current $I_{\rm ds}$ and of the gate–source capacitance $C_{\rm gs}$ are the true sources of IMD. There they can be accurately described by a Taylor-series expansion to third degree around the bias point $(V{\rm gs}_{\rm DC}, V{\rm ds}_{\rm DC})$ [2]:

$$\begin{aligned}&{\rm Ids}(V{\rm gs}, V{\rm ds})\\&\quad = {\rm Ids}_{\rm DC} + Gm\cdot v{\rm gs} + G{\rm ds}\cdot v{\rm ds} + Gm2\cdot v{\rm gs}^2\\&\qquad + Gmd\cdot v{\rm gs}\cdot v{\rm ds} + Gd2\cdot v{\rm ds}^2 + Gm3\cdot v{\rm gs}^3\\&\qquad + Gm2d\cdot v{\rm gs}^2\cdot v{\rm ds} + Gmd2\cdot v{\rm gs}\cdot v{\rm ds}^2 + Gd3\cdot v{\rm ds}^3 \quad (1)\\&C{\rm gs}(V{\rm gs})\\&\quad = C{\rm gs}_{\rm DC} + Cg2\cdot v{\rm gs} + Cg3\cdot v{\rm gs}^2. \quad (2)\end{aligned}$$

It has been observed many times that in a well-designed class-A amplifier, $Gm2$ and $Gm3$ are the dominant coefficients. That is the reason why a great effort was made to reduce them, by proper bias-point selection or in the foundry field, by an appropriate device's channel-doping control.

Bias-point control is generally driven either by optimized large-signal performance, which leads to the geometrical midpoint of the rectangle defined by $(I_{\rm ds} = 0, V_{\rm ds} = V{\rm ds}_{\rm Sat})$ and $(I_{\rm ds} = I{\rm ds}_{\rm Max}, V_{\rm ds} = V{\rm ds}_{\rm Breakdown})$, or by a careful search of the so-called IMD sweet spots [4], [5].

MESFET channel-doping control enabled the optimization of the device's nonlinearity itself, as was shown by Williams and Shaw [6] and Pucel [7]. In [6] and [7], a theoretical result was used to demonstrate the influence of doping profile on GaAs MESFET IMD performance. Pucel proposed the ideal IMD-free cubic or spike profiles, while Williams *et al.* also experimentally confirmed the superior linearity of a retrograde exponential profile, compared to the traditional uniform profile. From that point, the influence of various doping-profile patterns was tested or simply modeled, which included decreasing dopant concentration toward the substrate (normal negative slope) or retrograde doping (positive slope) [6], [8]–[10], Gaussian doping [8]–[10], and spike, step, or delta doping profiles [6], [11]–[14].

However, almost all of these measurement or modeling procedures suffer from two important problems which limit the range of applicability of their conclusions. The first one consists in mixing MESFET small-signal IMD with the distortion observed on very large-signal regimes. This kind of IMD is due to the above-referred strong nonlinearities, and thus cannot be directly correlated with the device's channel-doping profile. That is clearly the case of the transition between the triode and saturation regions, and gate–channel Schottky-junction forward conduction or breakdown. The second problem is related to the validity of analytical models based on the depletion-region approximation. In those cases, Debye length

Manuscript received August 22, 1995; revised July 18, 1997. This work was supported in part by Junta Nacional de Investigação Científica-JNICT, under the LIRA project.

The author is with the Instituto de Telecominicações, Universidade de Aveiro, 3800 Aveiro, Portugal.

Publisher Item Identifier S 0018-9480(97)08018-6.

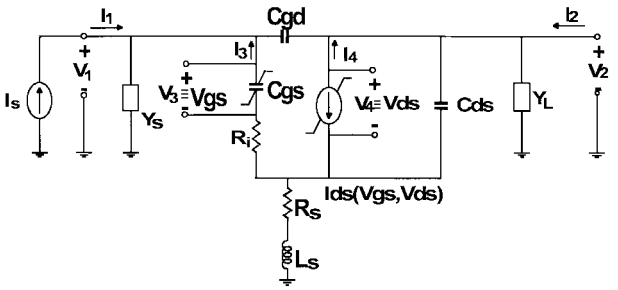

Fig. 1. Amplifier-circuit schematic for IMD calculations.

restrictions dramatically limit the usefulness of the conclusions drawn from certain ideal doping profiles that include too steep slopes.

Besides the achievements obtained with these specially tailored channel-doping profiles, some very good results of distortion performance observed in amplifiers based on general-purpose MESFET's (biased in a IMD sweet-spot) have recently been published [5], [15], which opens a promising field of study. The initial purpose of this paper is to provide a theoretical justification for these encouraging experiments and the necessary analysis for the control of their physical origins.

II. Theoretical Background

In this paper, a compromise between accuracy and simplicity is adopted by using an equivalent circuit model, like the one depicted in Fig. 1, where the nonlinear elements, $I\mathrm{ds}(V\mathrm{gs}, V\mathrm{ds})$ and $C\mathrm{gs}(V\mathrm{gs})$ are described by (1) and (2), and whose coefficients are obtained from an approximate physics-based analytical model. (The input and output parasitics pertaining to the extrinsic MESFET are assumed to be included in source and load admittances, respectively).

In linear-amplifier applications, the MESFET is biased, and for all range-of-signal excursions always maintained comfortably inside the $V\mathrm{ds}$ saturation region. There the MESFET channel can be divided in two regions [16]: the linear region, which is near the source and where an ohmic dependence of current density on electric field applies, and the saturation region, is close to the channel's drain end where free electrons move with their saturated velocity v_s.

Using a two-dimensional (2-D) analysis, Yamaguchi and Kodera [17] have shown that although charge carrier-density contour lines are not absolutely horizontal, the equivalent active-channel height h is almost constant along the saturated channel and independent on drain bias. This is a very important conclusion, as it allows an approximate one-dimensional (1-D) description of drain–source current control by the applied gate–channel voltage V, such that

$$I\mathrm{ds} = q \cdot v_s \cdot W \cdot \int_0^{A+As} n(y) \cdot dy \tag{3}$$

where W is the channel's cross-section width (along zz-axis) and A, As are the doped channel and substrate thickness (along yy-axis), respectively. The free electron density $n(y)$ must be determined by solving the 1-D Poisson equation in conjunction with the drift-diffusion current-density equilibrium equation, which relate $n(y)$, the potential variation across the channel $\psi(y)$, and the channel-doping profile $N_D(y)$ [16], [17]. However, this type of numerical analysis provides little directly useful information in terms of the sought relation between IMD and doping profile, since the exponential dependence of $n(y)$ on $\psi(y)$ imposed by the drift-diffusion equilibrium current-density equation, makes the Poisson equation an analytically intractable nonlinear differential equation.

An alternative approach was proposed by Yamagushi *et al.* [17] and Khatibzadeh *et al.* [16] which consists of an *a priori* assumption of the free electron-density functional form:

$$n(y) = T[h(V), y] \cdot N_D(y) \tag{4}$$

where $T[h(V), y]$ is a transition function, dependent on the equivalent channel height $h(V)$, and the extrinsic Debye length $\lambda_D = \sqrt{\varepsilon \cdot kT/(q^2 \cdot N_D)}$. $h(V)$ can then be determined by comparing $I\mathrm{ds}$ current resulting from the substitution of (4) on (3), with the one ideally obtained from a model based on the depletion-region approximation. In such a model, the dependence of $n(y)$ on $\psi(y)$ is neglected, thus assuming abrupt transitions from the depletion layer $(n(y) = 0, 0 < y < A - h(V))$ to the active channel $(n(y) = N_D^*(y), A - h(V) < y < A)$, and from this to the undoped substrate (or buffer layer) $(n(y) = 0, A < y < A + As)$:

$$\begin{aligned} I\mathrm{ds} &= q \cdot v_s \cdot W \cdot \int_0^{A+As} T[h(V), y] \cdot N_D(y) \cdot dy \\ &= q \cdot v_s \cdot W \cdot \int_{A-h(V)}^{A} N_D^*(y) \cdot dy. \end{aligned} \tag{5}$$

In this expression, $N_D^*(y)$ is the effective or apparent doping profile, as defined by Johnson *et al.* [18], which comes directly from a traditional differential-capacitance measurement technique. Numerical solutions of the Poisson and drift-diffusion equations [18], [19] have shown that as long as dependence of active-channel and depletion-layer heights $h(V)$, $d(V) = A - h(V)$, on gate–channel modulation voltage variations is concerned, the apparent doping profile $N_D^*(y)$ may be approximated by the real profile $N_D(y)$, provided $N_D(y)$ presents level transitions that span by at least the depletion-to-neutral channel-transition width $6\lambda_D$ [16], [17].

Therefore, the analytical procedure provided by the depletion approximation can be used to describe the drain–source current control by the gate–source voltage $V\mathrm{gs}$, but its results will have a validity limited to intermediate gate voltage's values that produce equivalent depletion-layer edges comfortably away either from both the gate–channel and the channel–substrate interfaces (roughly $V: 3 \cdot \lambda_D < d(V) < A - 6 \cdot \lambda_D$), or from any fast transition exhibited by the channel-doping profile. The first boundary case is not believed to produce a dramatic practical impact because in that zone of forward gate bias, the nonlinearity associated with the gate–channel Schottky junction conduction will dominate IMD performance. However, near the substrate (or buffer layer), the observed FET's behavior is the well-known soft pinchoff effect, which is similar in nature to what would happen near any other fast doping level variation, e.g., in step- or pulse-doped channels.

In conclusion, bearing in mind this validity analysis associated with the depletion-approximation model, one can simplify the Poisson equation by assuming that the charge is totally due to the completely ionized atoms present in a precisely defined depletion region located between the Schottky contact and $y = d(V)$. It has already been shown [6], [7] that the solution of this simplified Poisson equation, for an arbitrary equivalent doping profile $N_D(y)$ conjugated with (5), allows the calculation of the $I\mathrm{ds}(V\mathrm{gs})$ and $C\mathrm{gs}(V\mathrm{gs})$ coefficients by successive differentiation:

$$Gm = \frac{v_s \cdot W \cdot \varepsilon}{d(V)} \tag{6}$$

$$Gm2 = \frac{v_s \cdot W \cdot \varepsilon^2}{2 \cdot q} \cdot \frac{1}{d(V)^3} \cdot \frac{1}{N_D[d(V)]} \tag{7}$$

$$Gm3 = \frac{v_s \cdot W \cdot \varepsilon^3}{6 \cdot q^2} \cdot \frac{1}{d(V)^5} \cdot \frac{1}{N_D[d(V)]^3} \cdot [3 \cdot N_D[d(V)] + d(V) \cdot N_D'[d(V)]] \tag{8}$$

and

$$C\mathrm{gs} = \frac{W \cdot L \cdot \varepsilon}{d(V)} = Gm\frac{L}{v_s} \tag{9}$$

$$Cg2 = 2 \cdot Gm2\frac{L}{v_s}; Cg3 = 3 \cdot Gm3\frac{L}{v_s}. \tag{10}$$

From expressions equivalent to these, Pucel [7] derived two doping profiles that minimize the device's in-band distortion, i.e., produce low $Gm3$ and $Cg3$: $y^3 \cdot N_D(y) \to \infty$ or constant $y^3 \cdot N_D(y)$. The first condition, which cannot be precisely realized, and thus has been approximated by the spike doping [7], [11]–[14], reduces $Gm2$, and so its derivative $Gm3$. It can be seen from the relation of V and $d(V)$ that this doping profile makes depletion-region's height almost constant for a fairly wide range of gate biases. Therefore, it would be possible to produce a truly linear FET, i.e., one presenting transconductance and input capacitance independent on gate bias [13].

Even if this condition is not met, it is still possible to minimize third-order nonlinear distortion. This is done with a linear dependence of Gm on bias or, in other words, a constant $Gm2$. This is exactly what is meant by the second condition $y^3 \cdot N_D(y) =$ constant or $N_D(y) \propto y^{-3}$. It is easy to conclude that this condition constitutes the solution of the differential equation obtained from (8) for vanishing $Gm3$ and $Cg3$:

$$3 \cdot N_D(y) + y \cdot \frac{dN_D(y)}{dy} = 0. \tag{11}$$

III. Practical Considerations

From the device physics point of view, it should be clear that neither of the above conditions can be exactly obeyed for the whole range of gate biases. For example, as a real MESFET approaches pinchoff, it cannot present at that point (or in any other bias point) discontinuities in $I\mathrm{ds}$ or in any of its derivatives. It is known that $I\mathrm{ds}$ below the threshold region presents a constant value of zero, and then, due to the stated Debye length considerations, softly increases for higher values of $V\mathrm{gs}$. Therefore, it seems to be obvious that to guarantee the continuity of the function and all its derivatives, $Gm3$ must take some positive non-null value, at least in that zone. This discussion is really centered in the dependence of $Gm3$ on $V\mathrm{gs}$ bias $\delta^n Gm3/\delta V\mathrm{gs}^n$, which in a model like (1), would be represented by the magnitude of the higher order coefficients, $Gm4, Gm5, \cdots$. Bearing in mind the Volterra-series techniques for nonlinear circuit analysis [20], [21], it is easy to conclude that those higher order effects do not contribute to the third-order IMD products, which correspond to the device's low-level IMD performance. In conclusion, as long as high C/I ratios or other related nonlinear parameters as third-order intercept point IP_3 are concerned, it is not possible, nor it is strictly necessary, to have the above conditions verified for all ranges of gate biases, but at least one for a given quiescent point. It will be shown next that this situation is verified for some channel-doping profiles commonly encountered in commercially available general-purpose GaAs MESFET's, which allow them obvious advantages over the specially designed devices already proposed.

The first group of doping profiles considered describes the nth power doping:

$$N_D(y) = No \cdot (y - y_o)^n, \qquad y > 0 \text{ and } y > y_o. \tag{12}$$

Allowing y_o to get positive or negative values, this expression really shows great flexibility to model decaying $(n < 0)$, uniform $(n = 0)$, and retrograde $(n > 0)$ profiles. If y_o is positive, (12) will only give points of null $Gm3$ (i.e., will verify (11) for some y_c value) for $y_c = 3 \cdot y_o/2$ when $n = -1$, and for $(y_c = 3 \cdot y_o)$ when $n = -2$. If $y_o = 0$, then (12) will produce zero $Gm3$ for all y when $n = -3$ (Pucel's second condition [7]). Finally, if y_o is negative, (11) will present null $Gm3$ values for $y_c = 3 \cdot y_o/(3 + n)$ when $n < -3$.

The second group of profiles considered is the Gaussian doping, often used to describe devices prepared by ion implantation:

$$N_D(y) = No \cdot e^{-((y - y_o)/\sigma)^2}. \tag{13}$$

If $y_o \geq 0$, the Gaussian profile produces null $Gm3$ and $Cg3$ for $y_c = \frac{1}{2} \cdot [y_o + \sqrt{y_o^2 + 6 \cdot \sigma^2}]$, and if $y_o < 0, y_c = \frac{1}{2} \cdot [y_o + \sqrt{y_o^2 + 6 \cdot \sigma^2}]$, but now provided that $y_c > 0$.

The above discussion shows that there are certain parameters for these expressions capable of generating very good IMD regions, which should be observed for gate voltages such that $d(V) = y_c$.

Although actual channel-doping profiles may be originally conceived to match the ideal uniform, retrograde, step, delta, Gaussian patterns, etc., they always behave by ending up in soft transitions between different doping regions, e.g., in the channel to the intrinsic substrate or buffer-layer interface. Therefore, the apparent doping profiles $N_D^*(y)$ that must be used in the present analysis will present a greater complexity than the simple ideal starting forms. An interesting consequence of this is that a device with such a specially tailored doping profile will not be able to present the idealized IMD performance predicted from (6) to (10). Also, on the other

hand, it is possible to find $V_{\rm GS}$ bias points of null $Gm3$ and $Cg3$ in thin-channel general-purpose MESFET's (see Section V), which afford them third-order IMD performance comparable with the one actually obtained from those special devices.

IV. MESFET Intermodulation Distortion Calculations

In order to quantitatively evaluate the IMD performance improvement provided by one or the other alternative doping profile solutions, it is necessary to carefully study all contributions to nonlinear distortion in MESFET amplifiers. Although this is a task that has already been approximately performed for common MESFET devices, it is quite involved in this present situation due to the special nonlinear behavior that is being sought. In fact, it has been proven many times that in normal-operation, MESFET's third-order IMD is determined by the $I{\rm ds}(V{\rm gs})$ term involving $Gm3$, exactly the one that is now intended to produce a null effect. Thus, it should not be surprising that the majority of the approximations often followed can no longer apply, drawing of simple qualitative conclusions appear to be more difficult, and that an useful analysis requires careful nonlinear-device model extraction. Despite all of these associated problems, finding closed-form functions capable of describing IMD of an optimized MESFET amplifier provides two important features. First, it will allow a correct evaluation of the actual residual distortion that may be measured in such a particular (but also of very high practical interest) situation. Note that this remaining distortion will now take the first role in determining parameters such as C/I or IP_3, while the previous approximate analysis based only on $Gm3$ contribution would predict unrealistic IMD-free operation. Second, as the full analysis identifies the remaining IMD physical origins, it may also suggest ways for further improvements in the amplifier linearity.

The methodology followed in this paper uses the nonlinear currents method of the Volterra series [21], [22], and the amplifier-circuit description shown in Fig. 1. There it was assumed that all input and output parasitic elements pertaining to the FET's equivalent circuit model were included in the source $\boldsymbol{Ys}(\omega)$ and load $\boldsymbol{Y_L}(\omega)$ embedding impedances, respectively. It was also admitted that the only IMD generating elements were $C{\rm gs}(V{\rm gs})$ and $I{\rm ds}(V{\rm gs}, V{\rm ds})$, which is justified by the fact that in the saturation region, the other possible nonlinear element $Cgd(Vgd)$ is almost constant, thus behaving as a linear feedback capacitance.

Such an equivalent circuit model can be readily derived from device physics simulations by numerically differentiating $I{\rm ds}(V{\rm gs}, V{\rm ds})$ and $C{\rm gs}(V{\rm gs})$ results to obtain the series expansion's coefficients of (1) and (2). Alternatively, if a real device is being studied, an element-extraction procedure like the one proposed by Dambrine [23] should be used to obtain the equivalent circuit's linear-components values. Because measurement errors are magnified by numerical differentiation, laboratory extraction of $I{\rm ds}(V{\rm gs}, V{\rm ds})$ and $C{\rm gs}(V{\rm gs})$ expansions' coefficients becomes more delicate. For $I{\rm ds}(V{\rm gs}, V{\rm ds})$, Maas [1] and Pedro [2] proposed a direct extraction procedure based on small-signal harmonic–distortion measurements. However, no similar direct procedure has yet been presented for $C{\rm gs}(V{\rm gs})$ coefficients. This leaves us no other choice than to carefully differentiate smoothed $C{\rm gs}(V{\rm gs})$ data obtained from the successive application of Dambrine's method to a sufficiently large number of $V_{\rm GS}$ bias points.

The nonlinear current contributions of $C{\rm gs}$, $\boldsymbol{I}_3^{(n)}(\omega)$ and $I{\rm ds}, \boldsymbol{I}_4^{(n)}(\omega)$ can be related to the output $\boldsymbol{V}_2^{(n)}(\omega)$, and control voltages $V{\rm gs}^{(n)}(\omega) \equiv \boldsymbol{V}_3^{(n)}(\omega)$ and $\boldsymbol{V}{\rm ds}^{(n)}(\omega) \equiv \boldsymbol{V}_4^{(n)}(\omega)$ by the following set of equations:

$$\begin{bmatrix}\boldsymbol{V}_1\\ \boldsymbol{V}_2\\ \boldsymbol{V}_3\\ \boldsymbol{V}_4\end{bmatrix} = \begin{bmatrix}Z_{11} & Z_{12} & Z_{13} & Z_{14}\\ Z_{21} & Z_{22} & Z_{23} & Z_{24}\\ Z_{31} & Z_{32} & Z_{33} & Z_{34}\\ Z_{41} & Z_{42} & Z_{43} & Z_{44}\end{bmatrix} \times \begin{bmatrix}\boldsymbol{I}_1\\ \boldsymbol{I}_2\\ \boldsymbol{I}_3\\ \boldsymbol{I}_4\end{bmatrix}$$

$$\begin{aligned}\boldsymbol{I}_1 &= \boldsymbol{I}s\\ \boldsymbol{I}_2 &= 0\\ \boldsymbol{I}_3 &= j\omega \cdot Cg2 \cdot \boldsymbol{V}_3 * \boldsymbol{V}_3 + j\omega \cdot Cg3 \cdot \boldsymbol{V}_3 * \boldsymbol{V}_3 * \boldsymbol{V}_3\\ \boldsymbol{I}_4 &= Gm2 \cdot \boldsymbol{V}_3 * \boldsymbol{V}_3 + Gmd \cdot \boldsymbol{V}_3 * \boldsymbol{V}_4 + Gd2 \cdot \boldsymbol{V}_4 * \boldsymbol{V}_4\\ &\quad + Gm3 \cdot \boldsymbol{V}_3 * \boldsymbol{V}_3 * \boldsymbol{V}_3 + Gm2d \cdot \boldsymbol{V}_3 * \boldsymbol{V}_3 * \boldsymbol{V}_4\\ &\quad + Gmd2 \cdot \boldsymbol{V}_3 * \boldsymbol{V}_4 * \boldsymbol{V}_4 + Gd3 \cdot \boldsymbol{V}_4 * \boldsymbol{V}_4 * \boldsymbol{V}_4\end{aligned} \tag{14}$$

where the symbol * represents spectral convolution, and $\boldsymbol{I}s \equiv \boldsymbol{I}s(\omega)$ is an equal amplitude two-tone narrow-band excitation given by

$$i_s(t) = \frac{\boldsymbol{I}s_1}{2}e^{j\omega_1 t} + \frac{\boldsymbol{I}s_1^*}{2}e^{-j\omega_1 t} + \frac{\boldsymbol{I}s_2}{2}e^{j\omega_2 t} + \frac{\boldsymbol{I}s_2^*}{2}e^{-j\omega_2 t}. \tag{15}$$

Given that type of input signal, the following simplifications can be applied: $\boldsymbol{I}s_1 = \boldsymbol{I}s_2 = \boldsymbol{I}s; \omega_1 \approx \omega_2 \approx 2\omega_1 - \omega_2 \approx 2\omega_2 - \omega_1 \equiv \omega; \boldsymbol{Z}_{ij}(w_1) \approx \boldsymbol{Z}_{ij}(\omega_2) \approx \boldsymbol{Z}_{ij}(2\omega_1 - \omega_2) \approx \boldsymbol{Z}_{ij}(2\omega_2 - \omega_1) \approx \boldsymbol{Z}_{ij}(\omega)$ and $\Delta\omega \equiv \omega_1 - \omega_2 \ll \omega_1, \omega_2$. In order to obtain a useful analytical solution for this problem, it is necessary to consider some other simplifying assumptions in the FET's equivalent circuit: $Gm \cdot (Rs + j\omega \cdot Ls) \ll 1; \omega^2 \cdot {\rm Cgs}^2 \cdot Ri^2 \ll 1; j\omega \cdot Cgd \ll Gm$ and also $j\omega \cdot Cgd \ll (G{\rm ds} + j\omega \cdot C{\rm ds} + \boldsymbol{Y}_L(\omega))$.

In this situation, the expressions for the relevant Z-parameters became quite simple:

$$\boldsymbol{Z}_{21}(\omega) \approx -\frac{\boldsymbol{Z}o(\omega) \cdot Gm}{\boldsymbol{Y}(\omega)} \approx \boldsymbol{Z}_{23}(\omega) \tag{16}$$

$$\boldsymbol{Z}_{24}(\omega) \approx \boldsymbol{Z}o(\omega)\frac{\boldsymbol{Y}s(\omega) + j\omega \cdot C_T}{\boldsymbol{Y}(\omega)} \tag{17}$$

$$\boldsymbol{Z}_{31}(\omega) \approx \frac{1}{\boldsymbol{Y}(\omega)} \approx \boldsymbol{Z}_{33}(\omega) \tag{18}$$

$$\boldsymbol{Z}_{34}(\omega) \approx \boldsymbol{Z}o(\omega)\frac{j\omega \cdot Cgd}{\boldsymbol{Y}(\omega)} \tag{19}$$

$$\boldsymbol{Z}_{41}(\omega) \approx \boldsymbol{Z}_{21}(\omega) \quad \boldsymbol{Z}_{43}(\omega) \approx \boldsymbol{Z}_{23}(\omega) \quad \boldsymbol{Z}_{44}(\omega) \approx \boldsymbol{Z}_{24}(\omega)$$

with $C_T \equiv C{\rm gs} + Cgd$, $1/\boldsymbol{Z}o(\omega) = G{\rm ds} + j\omega \cdot C{\rm ds} + \boldsymbol{Y}_L(\omega)$ and $\boldsymbol{Y}(\omega) \equiv \boldsymbol{Y}s(\omega) + j\omega \cdot C_T + j\omega \cdot Cgd \cdot \boldsymbol{Z}o(\omega) \cdot Gm$.

The first-order control voltages are then

$$\boldsymbol{V}\mathrm{gs}^{(1)}(\omega) = \boldsymbol{Z}_{31}(\omega)\cdot\boldsymbol{Is}(\omega) \quad \text{and} \quad \boldsymbol{V}\mathrm{ds}^{(1)}(\omega) = \boldsymbol{Z}_{41}(\omega)\cdot\boldsymbol{Is}(\omega) \tag{20}$$

and thus, the second-order nonlinear current components that contribute to third-order IMD are

$$\boldsymbol{I}_3^{(2)}(2\omega) = 2j\omega\cdot Cg2\cdot\boldsymbol{Z}_{31}(\omega)^2\frac{\boldsymbol{Is}^2}{4} \tag{21}$$

$$\boldsymbol{I}_3^{(2)}(\Delta\omega) = j\Delta\omega\cdot Cg2\cdot|\boldsymbol{Z}_{31}(\omega)|^2\frac{|\boldsymbol{Is}|^2}{4}. \tag{22}$$

Given the narrow-band assumption $\Delta\omega \ll 2\omega$ the contribution of $\boldsymbol{I}_3^{(2)}(\Delta\omega)$ to third-order IMD may be neglected in comparison to the one due to $\boldsymbol{I}_3^{(2)}(2\omega)$. Therefore, $\boldsymbol{I}_3^{(2)}(\Delta\omega)\approx 0$:

$$\boldsymbol{I}_4^{(2)}(2\omega) = \Big[Gm2\cdot\boldsymbol{Z}_{31}(\omega)^2 + Gmd\cdot\boldsymbol{Z}_{31}(\omega)\cdot\boldsymbol{Z}_{41}(\omega) + Gd2\cdot\boldsymbol{Z}_{41}(\omega)^2\Big]\frac{\boldsymbol{Is}^2}{4} \tag{23}$$

$$\boldsymbol{I}_4^{(2)}(\Delta\omega) = \Big[2\cdot Gm2\cdot|\boldsymbol{Z}_{31}(\omega)|^2 + Gmd\cdot\boldsymbol{Z}_{31}(\omega)\cdot\boldsymbol{Z}_{41}(\omega)^* + Gmd\cdot\boldsymbol{Z}_{31}(\omega)^*\cdot\boldsymbol{Z}_{41}(\omega) + 2\cdot Gd2\cdot|\boldsymbol{Z}_{41}(\omega)|^2\Big]\frac{|\boldsymbol{Is}|^2}{4}. \tag{24}$$

The correspondent second-order control voltages become:

$$\boldsymbol{V}\mathrm{gs}^{(2)}(2\omega) = \boldsymbol{Z}_{33}(2\omega)\cdot\boldsymbol{I}_3^{(2)}(2\omega) + \boldsymbol{Z}_{34}(2\omega)\cdot\boldsymbol{I}_4^{(2)}(2\omega) \tag{25}$$

$$\boldsymbol{V}\mathrm{gs}^{(2)}(\Delta\omega) \approx \boldsymbol{Z}_{34}(\Delta\omega)\cdot\boldsymbol{I}_4^{(2)}(\Delta\omega) \tag{26}$$

$$\boldsymbol{V}\mathrm{ds}^{(2)}(2\omega) = \boldsymbol{Z}_{43}(2\omega)\cdot\boldsymbol{I}_3^{(2)}(2\omega) + \boldsymbol{Z}_{44}(2\omega)\cdot\boldsymbol{I}_4^{(2)}(2\omega) \tag{27}$$

$$V\mathrm{ds}^{(2)}(\Delta\omega) = \boldsymbol{Z}_{44}(\Delta\omega)\cdot\boldsymbol{I}_4^{(2)}(\Delta\omega). \tag{28}$$

Because of the obvious necessity to bias the drain terminal, and of the common practice to short circuit the FET at low frequencies in order to prevent parasitic oscillations, it is almost sure that the load impedance at the difference frequency $\boldsymbol{Z}_L(\Delta\omega)$ will be very low, which makes $\boldsymbol{Z}_{44}(\Delta\omega)\approx 0$ and $\boldsymbol{V}\mathrm{ds}^{(2)}(\Delta\omega)\approx 0$. Furthermore, the admittance of Cgd at $\Delta\omega$ will also be very low, making $\boldsymbol{Z}_{34}(\Delta\omega)\approx 0$, and thus, $\boldsymbol{V}\mathrm{gs}^{(2)}(\Delta\omega)\approx 0$. The combination of these two conditions implies that in a normal narrow-band microwave amplifier, the only second-order product that can produce significant contribution to in-band third-order IMD is the one at the second harmonic 2ω.

Accordingly, third-order nonlinear-current components at $2\omega_1-\omega_2$ (or $2\omega_2-\omega_1$) will be in compact form:

$$\begin{aligned}\boldsymbol{I}_3^{(3)}(2\omega_1-\omega_2) &= 2j\omega\cdot Cg2\cdot\boldsymbol{Z}_{31}(\omega)^*\\ &\quad\cdot\Big[\boldsymbol{Z}_{33}(2\omega)\cdot\boldsymbol{I}_3^{(2)}(2\omega)+\boldsymbol{Z}_{34}(2\omega)\cdot\boldsymbol{I}_4^{(2)}(2\omega)\Big]\frac{\boldsymbol{Is}^*}{2}\\ &\quad+3j\omega\cdot Cg3\cdot\boldsymbol{Z}_{31}(\omega)\cdot|\boldsymbol{Z}_{31}(\omega)\cdot|^2\frac{\boldsymbol{Is}\cdot|\boldsymbol{Is}|^2}{8}\end{aligned} \tag{29}$$

$$\begin{aligned}\boldsymbol{I}_4^{(3)}(2\omega_1-\omega_2) &= 2\cdot Gm2\cdot\boldsymbol{Z}_{31}(\omega)^*\\ &\quad\cdot\Big[\boldsymbol{Z}_{33}(2\omega)\cdot\boldsymbol{I}_3^{(2)}(2\omega)+\boldsymbol{Z}_{34}(2\omega)\cdot\boldsymbol{I}_4^{(2)}(2\omega)\Big]\frac{\boldsymbol{Is}^*}{2}\\ &\quad+Gmd\cdot\boldsymbol{Z}_{31}(\omega)^*\\ &\quad\cdot\Big[\boldsymbol{Z}_{43}(2\omega)\cdot\boldsymbol{I}_3^{(2)}(2\omega)+\boldsymbol{Z}_{44}(2\omega)\cdot\boldsymbol{I}_4^{(2)}(2\omega)\Big]\frac{\boldsymbol{Is}^*}{2}\\ &\quad+Gmd\cdot\boldsymbol{Z}_{41}(\omega)^*\\ &\quad\cdot\Big[\boldsymbol{Z}_{33}(2\omega)\cdot\boldsymbol{I}_3^{(2)}(2\omega)+\boldsymbol{Z}_{34}(2\omega)\cdot\boldsymbol{I}_4^{(2)}(2\omega)\Big]\frac{\boldsymbol{Is}^*}{2}\\ &\quad+2\cdot Gd2\cdot\boldsymbol{Z}_{41}(\omega)^*\\ &\quad\cdot\Big[\boldsymbol{Z}_{43}(2\omega)\cdot\boldsymbol{I}_3^{(2)}(2\omega)+\boldsymbol{Z}_{44}(2\omega)\cdot\boldsymbol{I}_4^{(2)}(2\omega)\Big]\frac{\boldsymbol{Is}^*}{2}\\ &\quad+\Big[3\cdot Gm3\cdot\boldsymbol{Z}_{31}(\omega)\cdot|\boldsymbol{Z}_{31}(\omega)|^2\\ &\qquad+Gm2d\cdot\boldsymbol{Z}_{31}(\omega)^2\cdot\boldsymbol{Z}_{41}(\omega)^*\\ &\qquad+2\cdot Gm2d\cdot|\boldsymbol{Z}_{31}(\omega)|^2\cdot\boldsymbol{Z}_{41}(\omega)\\ &\qquad+Gmd2\cdot\boldsymbol{Z}_{31}(\omega)^*\cdot\boldsymbol{Z}_{41}(\omega)^2\\ &\qquad+2\cdot Gmd2\cdot\boldsymbol{Z}_{31}(\omega)\cdot|\boldsymbol{Z}_{41}(\omega)|^2\\ &\qquad+3\cdot Gd3\cdot Z_{41}(\omega)\cdot|Z_{41}(\omega)|^2\Big]\frac{\boldsymbol{Is}\cdot|\boldsymbol{Is}|^2}{8}\end{aligned} \tag{30}$$

and finally, the IMD output-voltage component:

$$V_2^{(3)}(2\omega_1-\omega_2) = \boldsymbol{Z}_{43}(\omega)\cdot\boldsymbol{I}_3^{(3)}(2\omega_1-\omega_2)+\boldsymbol{Z}_{44}(\omega)\cdot\boldsymbol{I}_4^{(3)}(2\omega_1-\omega_2). \tag{31}$$

As this result is fully analytical, it can be used to extract some qualitative conclusions on the possible improvement that may be obtained by making $Gm3=0, Cg3=0$ (doping profile with an IMD optimum point) or alternatively $Gm3=0, Cg3=0$ and $Gm2=0, Cg2=0$ (special case of ideal spike- or step-doped channel). For that, it is first necessary to have ideas of the sign and magnitude of the $I\mathrm{ds}(V\mathrm{gs}, V\mathrm{ds})$ and $C\mathrm{gs}(V\mathrm{gs})$ coefficients.

Real $I\mathrm{ds}$ coefficients' values were extracted from a commercially available 300-μm GaAs MESFET, with the VHF harmonic–distortion measurements procedure described by Pedro [2], while $C\mathrm{gs}$ coefficients' values were obtained by successive differentiation of $C\mathrm{gs}(V\mathrm{gs})$ data extracted from measured S-parameters. The obtained values for $V\mathrm{gs}_{\mathrm{DC}} = -0.25$ V, $V\mathrm{ds}_{\mathrm{DC}} = 3$ V are as follows:

$$\begin{aligned} Gm &= 70\ \text{mS}\\ G\mathrm{ds} &= 6.5\ \text{mS}\\ Gm2 &= 12\ \text{mS/V}\\ Gmd &= -0.3\ \text{mS/V}\\ Gd2 &= -0.33\ \text{mS/V}\\ Gm3 &= 0.0\ \text{mS/V}^2\\ Gm2d &= -0.7\ \text{mS/V}^2\\ Gmd2 &= -0.083\ \text{mS/V}^2\\ Gd3 &= 0.086\ \text{mS/V}^2\\ C\mathrm{gs} &= 0.35\ \text{pF}\\ Cg2 &= 0.06\ \text{pF/V}\\ Cg3 &= 0.0\ \text{pF/V}^2. \end{aligned}$$

TABLE I
EVALUATION OF VARIOUS COEFFICIENTS' CONTRIBUTIONS IN A PRACTICAL MESFET AMPLIFIER

	Y_S, Y_L for Max Gain		Y_S, Y_L for Max Output Power	
Output Voltage Contribution	Mag[$V_{2\,IMD}$]	Ang[$V_{2\,IMD}$]	Mag[$V_{2\,IMD}$]	Ang[$V_{2\,IMD}$]
Vout(ω)	0.74 V	165 °	0.41 V	149 °
Cg2	7.22 x 10^{-5} V	-50 °	6.61 x 10^{-5} V	-77 °
Cg3	1.01 x 10^{-3} V	-81 °	5.05 x 10^{-4} V	-102 °
Gm2	1.41 x 10^{-4} V	8 °	1.25 x 10^{-4} V	-10 °
Gmd	6.78 x 10^{-6} V	-18 °	3.56 x 10^{-6} V	37 °
Gd2	5.12 x 10^{-5} V	65 °	2.15 x 10^{-5} V	-66 °
Gm3	3.52 x 10^{-3} V	-23 °	1.72 x 10^{-3} V	-35°
Gm2d	7.57 x 10^{-4} V	163 °	2.00 x 10^{-4} V	147 °
Gmd2	5.14 x 10^{-4} V	-12 °	7.11 x 10^{-5} V	-31 °
Gd3	3.17 x 10^{-3} V	-7 °	2.22 x 10^{-4} V	-29 °
1st Total (Gm3=-18mS/V^2, Cg3=-0.05pF/V^2)	7.04 x 10^{-3} V	-22 °	2.44 x 10^{-3} V	-47 °
2nd Total (Gm3=0, Cg3=0)	3.15 x 10^{-3} V	4 °	2.75 x 10^{-4} V	-31 °
3rd Total (Gm2=Gm3=0, Cg2=Cg3=0)	2.74 x 10^{-3} V	-10 °	8.67 x 10^{-5} V	-23 °
4th Total	1.56 x 10^{-3} V	55 °	5.90 x 10^{-5} V	48 °

With these typical values it seems that third-order IMD contributions (arising from second-degree coefficients) will be about one order of magnitude below the contributions due to third-degree terms. That conclusion has important practical implications in the way that it discourages further amplifier IMD optimization by second harmonic-terminations tuning, unless some other measures are first taken to reduce the third-degree coefficients' contributions. Therefore, our attention should now concentrate on the term of $\boldsymbol{I}_3^{(3)}$ involving $Cg3$ and the last term of $\boldsymbol{I}_4^{(3)}$.

In an usual amplifier design where both input and output ports will be tuned, $\boldsymbol{Y}(\omega)$ and $\boldsymbol{Z}o(\omega)$ are nearly real, making all $\boldsymbol{Z}_{ij}$ parameters—except $\boldsymbol{Z}_{34}(\omega)$—also approximately real. Therefore, we may expect possible compensations between the terms of $Gm3$, $Gm2d$, $Gmd2$, and $Gd3$ because of their relative signs. IMD due to $Cg3$ tends to appear at the output in quadrature in these contributions, and thus, it cannot be reduced.

These possible compensations will be mainly dependent on the magnitude of the $\boldsymbol{Z}_{41}(\omega)/\boldsymbol{Z}_{31}(\omega)$ ratio, which is approximately the device's voltage gain $\boldsymbol{V}\mathrm{ds}(\omega)/\boldsymbol{V}\mathrm{gs}(\omega)$. Thus, voltage-gain control via appropriate $\boldsymbol{Z}_L(\omega)$ selection can be used to optimize amplifier IMD [2]. Another interesting possibility to be explored consists of having a $Gm3$ slightly different from zero, which would even enable the compensation of other coefficients' contributions. In that sense, it seems it could be better to have a MESFET with a doping profile that produces a zero-crossing $Gm3$, rather than one presenting a broad range of $V\mathrm{gs}$ for which $Gm3 = 0$, since it would provide control over that coefficient's magnitude and sign by fine tuning of V_{GS} bias [5].

Although the above conclusions have been drawn from a simplified model, they can be generalized for practical cases, as is shown in Table I. In this table, we describe results obtained at 2 GHz with the complete equivalent circuit model of Fig. 1, using the coefficients' values already indicated. Two different load conditions were selected: $\boldsymbol{Y}_L(\omega)$ for maximum gain (first two columns), and for maximum output signal power (third and fourth columns). In both cases, input termination was simply chosen to produce source matching, since in-band unconditionally stable operation was guaranteed by input resistive loading. These two examples are illustrative of practical designs for low-level–high-dynamic range, and low-distortion–high-output power amplifiers, respectively.

All rows represent output voltage values (magnitude and phase) taken at the fundamental $\boldsymbol{V}_2^{(1)}(\omega)$ and IMD $\boldsymbol{V}_2^{(3)}(2\omega_1 - \omega_2)$ for equal-output signal power. Because of the interactions that are verified between second-order contributions to produce products of third order, all values attributed to second-degree terms were calculated assuming that all the other second-degree coefficients were present. That was not necessary for the third-degree terms, and so those values were obtained with all coefficients set to zero, except the one under study. The voltages corresponding to $Gm3$ or $Cg3$ have only comparison purposes, and were calculated using values associated with a slightly lower gate bias: $V\mathrm{gs}_{\mathrm{DC}} = -0.5$ V: $Gm3 = -18$ mS/V^2, $Cg3 = -0.05$ pF/V^2.

To evaluate the IMD improvement that one may expect from vanishing $Gm3$ and $Cg3$, and also $Gm2$ and $Cg2$, four different totals were calculated for each termination's condition. In this example, the IMD improvement gained by setting $Gm3 = 0$ and $Cg3 = 0$ (7 or 19 dB) is obvious from the individual values of their contributions. Note however, that in the high-gain example the relatively high contribution of $Gd3$, which obviates more impressive differences in the totals, is due to the high voltage gain induced by the output matching condition. In the power amplifier case, where $\boldsymbol{Y}_L(\omega)$ was selected for power requirements (not maximum gain), the voltage gain is lower, and therefore, much higher improvements resulted. By observing the first, second, and third totals, it can be concluded that the advantage of having a special FET with an approximately constant Gm (in comparison to another common device with only one defined point of null $Gm3$), is approximately 10 dB for the output-power optimized example, but not very significant for the high-gain example (1.2 dB). Moreover, since that latter device

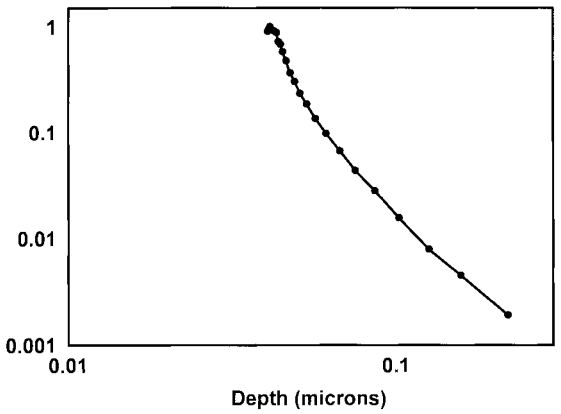

Fig. 2. Normalized doping profile $N_D^*(y)$ of general-purpose MESFET NE70083, obtained from measured ratio of $Gm^3/Gm2$.

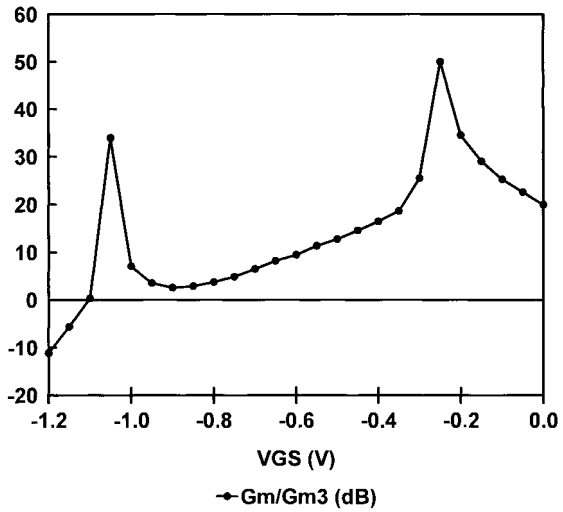

Fig. 3. Ratio of measured Gm and $Gm3$ of NE70083 showing the points of very good third-order IMD.

option allows the selection of convenient non-null $Gm3$ and $Cg3$ ($Gm3 = +12$ mS/V^2, $Cg3 = +0.03$ pF/V^2—max gain and $Gm3 = +2.6$ mS/V^2, $Cg3 = +0.004$ pF/V^2—max output power) that produced the fourth total results (as theoretically predicted above), it seems that it could really represent a better choice for a low IMD amplifier application (6- or 13-dB improvement over the second totals).

V. Experimental Validation

Those theoretical results induced the study of real-world equivalent doping profiles, measured in general-purpose GaAs MESFET's, like the one shown in Fig. 2.

Using the approximation of this pattern by a piecewise combination of appropriate nth-power doping profiles like the ones given in (12), two different depletion-depth values corresponding to null $Gm3$ were predicted. As each of these depths has a $V_{\rm GS}$-bias voltage counterpart, it was anticipated that this device should present two distinct bias points of very good IMD performance. That was truly confirmed by the direct laboratory extraction of Gm and $Gm3$ from S-parameters and harmonic measurements [2].

Fig. 3 shows the nonlinear characterization results thus obtained. It presents the ratio of $Gm/Gm3$ (which is generally taken as a figure of merit (FOM) of the device's linearity) for the whole range of negative gate bias. The observation of this figure leads to the conclusion that this MESFET really shows two points of high $Gm/Gm3$ corresponding to two $V_{\rm GS}$ values of null $Gm3$. The first $Gm3$ null is located at $V_{\rm GS} = -1.05$ V, near the FET's threshold voltage where Gm is very small. This is a point of little practical interest for linear power amplification, because of its low associated gain. However, the second $Gm3$ null stands for $V_{\rm GS} = -0.25$ V, i.e., in a zone of high transconductance. Thus, contrary to the former, this latter $Gm3$ null constitutes a quiescent point of great importance as it may be used to build low IMD amplifiers.

To prove that, another similar device was characterized and used in a common single-stage S-band amplifier. Fig. 4 represents the simplified schematic of the implemented amplifier.

The circuit was then submitted to a conventional two-tone test. Measured results obtained with that experiment are plotted in Figs. 5 and 6. Also plotted in these figures are simulated results obtained with the Volterra-series model discussed in the previous section.

Fig. 5 describes predicted and observed sensitivity of third-order IMD output power on gate bias. It really confirms the predicted two $V_{\rm GS}$-bias zones of good linearity, one near the device's pinchoff ($V_T \approx -1.6$ V), and another in a region of more useful class-A operation's quiescent points. Inside the normal zone of bias, i.e., for $I_{\rm DS}$ currents ranging from 20% to 100% Idss, an IMD output power variation of more than 20 dB could be measured.

On the other hand, Fig. 6 shows a 1-dB compression point of 12 dBm and an extrapolated third-order intercept point IP_3 of 36 dBm. The departure from simulated to measured results observed on the fundamental and IMD output powers for the highest input levels is due to the third-order restriction imposed on the adopted Volterra model. The observed $P_{1\,\rm dB}$ and IP_3 figures are thought to be remarkable results for a general-purpose MESFET biased with $V_{\rm ds} = 3.0$ V and $I_{\rm ds} = 40$ mA. In fact, they correspond to FOM's of $IP_3/P_{\rm DC} = 33$ and $IP_3/P_{1\,\rm dB} = 24$ dB, which compare to the $IP_3/P_{\rm DC} = 3.7$ and $IP_3/P_{1\,\rm dB} = 14$ dB published for a conventional power-MESFET amplifier, and to $IP_3/P_{\rm DC} = 50$ and $IP_3/P_{1\,\rm dB} = 14$ dB obtained with a MESFET device with a spike-doped channel [14].

VI. Conclusions

A different point of view on the MESFET linearity dependence on doping profile was presented. It led to the interesting conclusion that good IMD performance may be expected from a MESFET with no specialized doping profile if its channel-doping pattern is carefully studied and the $V_{\rm GS}$ bias point precisely selected.

Two-tone test results observed on a practical amplifier proved that the present procedure indeed produces linearity FOM's that are much better than obtained with conventional power FET's, and can even approximate the FOM's of specially tailored devices.

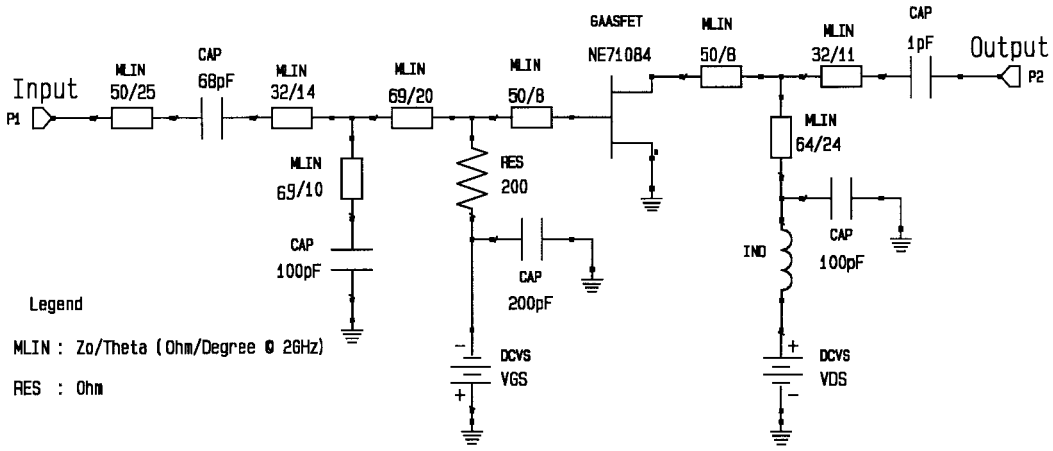

Fig. 4. Simplified schematic diagram of the implemented S-band amplifier.

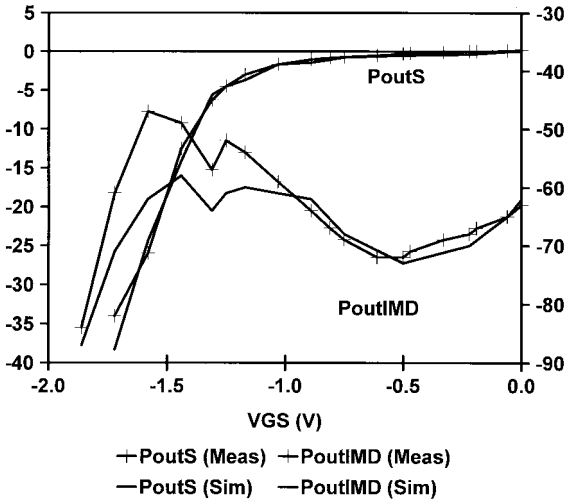

Fig. 5. Measured and simulated results of IMD output power sensitivity on gate-bias voltage.

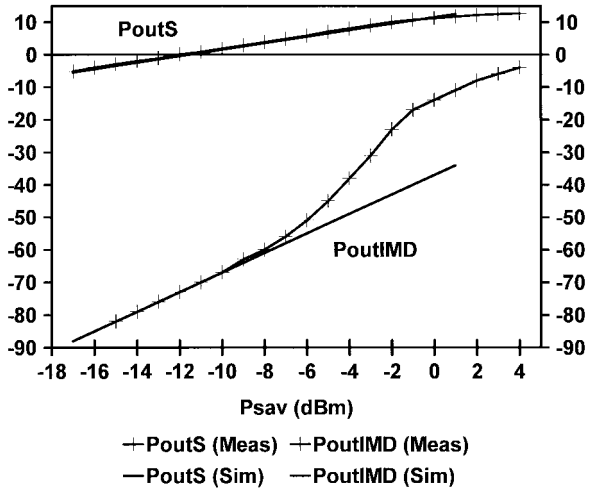

Fig. 6. Measured and simulated results of output power at the fundamental and third-order IMD and implemented amplifier.

ACKNOWLEDGMENT

The author would like to thank L. Ramos Gomes for the implementation and test of the experimental prototype.

REFERENCES

[1] S. Maas and A. Crosmun, "Modeling the gate I/V characteristic of a GaAs MESFET for Volterra-series analysis," *IEEE Trans. Microwave Theory Tech.*, vol. 37, pp. 1134–1136, July 1989.

[2] J. Pedro and J. Perez, "Accurate simulation of GaAs MESFET's intermodulation distortion using a new drain–source current model," *IEEE Trans. Microwave Theory Tech.*, vol. 42, pp. 25–33, Jan. 1994.

[3] S. A. Maas, "A general-purpose computer program for the Volterra-series analysis of nonlinear microwave circuits," in *1988 IEEE Int. Microwave Theory Tech. Symp. Dig.*, New York, June 1988, pp. 311–314.

[4] R. Vaitkus, V. Nair, and S. Tehrani, "A low-current linearity sweet spot in HFET's," in *IEEE Int. Microwave Theory Tech. Symp. Dig.*, Orlando, FL, May 1995, pp. 523–526.

[5] J. Pedro and J. Perez, "On the bias point selection for improved performance in low intermodulation distortion amplifiers," in *Proc. European GAAS Symp.*, Torino, Italy, Apr. 1994, pp. 353–355.

[6] R. Williams and D. Shaw, "Graded channel FET's: Improved linearity and noise figure," *IEEE Trans. Electron Devices*, vol. ED-25, pp. 600–605, June 1978.

[7] R. Pucel, "Profile design for distortion reduction in microwave field effect transistors," *Electron. Lett.*, vol. 14, pp. 204–206, Mar. 1978.

[8] J. Higgins, "Modeling the influence of carrier profiles on MESFET characteristics," *IEEE Trans. Electron Devices*, vol. 27, pp. 1066–1073, June 1980.

[9] J. Higgins, R. Kuvas, F. Eisen, and D. Ch'en, "Low-noise GaAs FET's prepared by ion implantation," *IEEE Trans. Electron Devices*, vol. ED-25, pp. 587–596, June 1978.

[10] J. Higgins and R. Kuvas, "Analysis and improvement of intermodulation distortion in GaAs power FET's," *IEEE Trans. Microwave Theory Tech.*, vol. MTT-28, pp. 9–17, Jan. 1980.

[11] J. Dekkers, F. Ponse, and H. Beneking, "Buried channel GaAs MESFET's—Scattering parameter and linearity dependence on the channel doping profile," *IEEE Trans. Electron Devices*, vol. ED-28, pp. 1065–1070, Sept. 1981.

[12] H. Beneking, A. Cho, J. Dekkers, and H. Morkoç, "Buried-channel GaAs MESFET's on MBE material: Scattering parameters and intermodulation signal distortion," *IEEE Trans. Electron Devices*, vol. ED-29, pp. 811–813, May 1982.

[13] T. Tan, K. Kotzebue, D. Braun, J. Centanni, and D. Mcquate, "A low-distortion K-band GaAs power FET," *IEEE Trans. Microwave Theory Tech.*, vol. 36, pp. 1023–1032, June 1988.

[14] S. Chu, J. Huang, W. Struble, G. Jackson, N. Pan, M. J. Schindler, and Y. Tajima, "A highly linear MESFET," in *IEEE Int. Microwave Theory Tech. Symp. Dig.*, Boston, MA, June 1991, pp. 725–728.

[15] J. Pedro and J. Perez, "Design techniques for low intermodulation distortion amplifiers," *Microwave J.*, vol. 37, no. 5, pp. 94–104, May 1994.

[16] M. Khatibzadeh and R. Trew, "A large-signal, analytic model for the GaAs MESFET," *IEEE Trans. Microwave Theory Tech.*, vol. 36, pp. 231–238, Feb. 1988.

[17] K. Yamaguchi and H. Kodera, "Drain conductance of junction gate FET's in the hot electron range," *IEEE Trans. Electron Devices*, vol. ED-23, pp. 545–553, June 1976.

[18] W. Johnson and P. Panousis, "The influence of Debye length on the C-V measurement of doping profiles," *IEEE Trans. Electron Devices*, vol. ED-18, pp. 965–973, Oct. 1971.
[19] P. Gray, D. DeWitt, A. Boothroyd, and J. Gibbons, *Physical Electronics and Circuit Models of Transistors*. New York: Wiley, 1964.
[20] D. Weiner and J. Spina, *Sinusoidal Analysis and Modeling of Weakly Nonlinear Circuits*. New York: Van Nostrand, 1980.
[21] S. A. Maas, *Nonlinear Microwave Circuits*. Norwood, MA: Artech House, 1988.
[22] J. Bussgang, L. Ehrman, and J. Graham, "Analysis of nonlinear systems with multiple inputs," *Proc. IEEE*, vol. 62, pp. 1088–1119, Aug. 1974.
[23] G. Dambrine, A. Cappy, F. Heliodore, and E. Playez, "A new method for determining the FET small-signal equivalent circuit," *IEEE Trans. Microwave Theory Tech.*, vol. 36, pp. 1151–1159, July 1988.

José Carlos Pedro (S'90–M'95) was born in Espinho, Portugal, on March 7, 1962. He received the diploma and doctoral degrees in electronics and telecommunications engineering from the University of Aveiro, Aveiro, Portugal, in 1985 and 1993, respectively.

From 1985 to 1993, he was an Assistant Lecturer at the University of Aveiro. Since 1993, he has been a Professor, and is currently the head of the Radio Frequency Group, Instituto de Telecomunicações. His main scientific research interests include active device modeling and the analysis and design of various nonlinear microwave and optoelectronics circuits, in particular, the design of highly linear multicarrier power amplifiers.

Dr. Pedro received the Marconi Young Scientist Award in 1993.